Electroreduction of μ-Oxo Iron(III) Porphyrins Adsorbed on an Electrode Leading to a Cofacial Geometry for the Iron(II) Complex: Unexpected Active Site for the Catalytic Reduction of O_2 to H_2O

Kenichi Oyaizu, Agus Haryono, Junichiro Natori, Hiroshi Shinoda, and Eishun Tsuchida[*,#]

Advanced Research Institute for Science and Engineering, Department of Polymer Chemistry, Waseda University, Tokyo 169-8555

(Received November 9, 1999)

Acidification of a solution of (μ-oxo)bis[(5,10,15,20-tetraphenylporphyrinato)iron(III)] ([{Fe(tpp)}$_2$O], **II**) in CH_2Cl_2 produced equimolar amounts of a hydroxoiron(III) complex [(tpp)Fe^{III}(OH)] (**III**) and an iron(III) complex [(tpp)Fe^{III}(ClO_4)] (**IV**). The complex **IV** was isolated as a perchlorate salt, which crystallyzed in the triclinic space group $P\bar{1}$ (#2); a = 11.909(3), b = 19.603(4), c = 10.494(3) Å, α = 95.74(2)°, β = 107.91(2)°, γ = 89.14(2)°, V = 2319.1(9) Å^3, Z = 2, D_{calc} = 1.328 g cm^{-3}, μ(Mo $K\alpha$) = 4.35 cm^{-1}, final R = 0.055 and R_w = 0.050. The crystal structure of **IV** revealed that ClO_4^- is coordinated to the iron atom, which may be driven by the preference of iron(III) to be five coordinate rather than four coordinate. Reduction of the complex **II** in the presence of acid by electrolysis and/or by a reducing agent, such as sodium dithionite, under argon produced [Fe^{II}(tpp)]. The addition of O_2 to a solution of [Fe(tpp)] in acidic CH_2Cl_2 in the presence of an equimolar amount of the reducing agent produced the complex **III**. When the complex **II** was adsorbed on an electrode surface and placed in aqueous acidic electrolyte solutions, electroreduction of the adsorbate proceeded according to the half-reaction:

[{Fe(tpp)}$_2$O] + 2H$^+$ + 2e$^-$ → 2[Fe(tpp)] + H_2O, at 0.031—0.059 pH **V** (vs. SCE, pH > 1.0). Based on these results, oxo-bridged iron(III) porphyrin dimers were used as electrocatalysts for the reduction of O_2. The catalytic reduction of O_2 proceeded at potentials in the vicinity of those for **II**. As a whole, the proportion of H_2O as the product increased from 50% for adsorbed [(tpp)Fe^{III}Cl] to > 90% for the adsorbed dimer. Thus, electroreduction of the dimer adsorbed on a carbon electrode immersed in aqueous acid produced two solid state, cofacially fixed iron(II) porphyrin molecules:

[PFe^{III}OFe^{III}P]$_{ad}$ + 2H$^+$ + 2e$^-$ → [PFe^{II} Fe^{II}P]$_{ad}$ + H_2O (P = porphyrin dianion). Coordination of molecular oxygen to the adjacent two iron(II) centers under acidic conditions allowed formation of O_2-bridged iron(III) porphyrin [PFe^{III}(O_2) Fe^{III}P]$_{ad}$ at the electrode surface. Electroreduction of the adsorbate under acidic conditions produced H_2O and allowed the reformation of [PFe^{II} Fe^{II}P]$_{ad}$. The implication is that the electroreduction of the adsorbed oxo-bridged dimer gives a cofacial geometry for PFe^{II} on the electrode, facilitating the coordination and subsequent splitting of O_2.

Recent extensive studies on the electroreduction of O_2 have evolved a wide variety of metal complexes that can be used as catalysts when immobilized at the electrode surface.[1] The catalyzed reaction can proceed by a two-electron pathway to produce H_2O_2 or by a net four-electron pathway to yield H_2O. The reductive cleavage of the O=O bond by a four-electron, four-proton reaction provides not only a clean energy-transformation process relevant to biological respiratory systems,[2] but also a redox system for the O_2-oxidative polymerization of organic molecules.[3] Recent topics also involve the application of such catalysts to fuel cell technologies.[4] To enhance the rate of the electroreduction of O_2, metalloporphyrins have frequently been employed as catalysts. Typical examples are provided by mononuclear cobalt porphyrins[5] and iron porphyrins[6] which reduce O_2 to H_2O_2 predominantly. Dicobalt cofacial porphyrins[7] are among the few electrocatalysts which are able to promote the direct reduction of O_2 to H_2O by a four-electron mechanism in acidic media where an O_2 molecule coordinates to form a μ-O_2 bridge between the two cobalt centers, allowing subsequent scission of the O–O bond. Their results have demonstrated the importance of the geometry of porphyrins for the efficient electron transfer and cleavage of the O–O bond. However, the cofacial diporphyrin complexes are usually difficult to synthesize, and are only produced in low yield. An alternative to the cofacial diporphyrins has been provided by an ion complex, i.e., an electrostatic aggregate, of cationic *meso*-tetra(*N*-methyl-4-pyridyl)porphyrinatoiron(II) and anionic *meso*-tetra(*p*-sulfophenyl)porphyrinatoiron(II), which allowed a cofacial geometry of the porphyrin molecules.[8]

Herein we report that μ-oxo-bridged iron porphyrin dimers could be versatile and more convenient electrocatalysts for the four-electron reduction of O_2. Indeed, the reaction of O_2 with iron porphyrins is a vast area of research: autoxidation of simple iron(II) porphyrins in solution provides μ-oxo dimers according to the stoichiometry 4PFe^{II} + O_2 → 2PFe^{III}OFe^{III}P where P = porphyrin dianion.[9] It has been suspected that under certain circumstances O_2 can react

CREST investigator, JST.

with PFe^{II} to form a bridged PFeO$_2$FeP species which is subsequently cleaved to yield the oxoiron(IV) complex PFe^{IV}=O during the initial stages of the reaction.[10] On the other hand, we have found that electroreduction of PFe^{III}OFe^{III}P under acidic conditions produces PFe^{II} and H_2O, and that the electroreduction of adsorbed dimer could provide a cofacial geometry for PFe^{II} on the electrode. As a result, the proportion of H_2O as the reduced product increases significantly for the adsorbed dimer. In this report, a previous preliminary study[11] has been extended, and a possible mechanism for the catalytic four-electron electroreduction of O_2 is offered.

Results and Discussion

Synthesis and Crystal Structure of Iron Porphyrin Complexes. Electrochemical and structural studies of iron complexes with porphyrin ligands attract particular attention because of their reactivities toward molecular oxygen, allowing possible applications to electrocatalysts for oxygen reduction. The most abundant and important molecule in their isostructural family is the μ-oxo diiron(III) porphyrin. μ-Oxo dimers having tpp (**II**) and oep (**VI**) as ligand were prepared from the corresponding mononuclear porphyrinatoiron(III) chlorides **I** and **V**, respectively.[12,13] A comparison of the catalytic behavior of the two complexes has been made, because it was shown that the metal-metal distance is crucial in the ratio between the four- and two-electron reduction of O_2 (vide infra). Structurally, iron(III) atoms are in a square-pyramidal five-coordination arrangement and deviate from the porphyrin least-squares plane by as much as 0.495 Å. Indeed, the coordination geometry around iron(III) is an important issue when the catalytic mechanism for the reduction of O_2 is discussed later.

We previously reported that the electroreduction of oxo-metal complexes (O=M^X(L), L = ligand), such as VO(salen) (H_2salen = *N*,*N*′-ethylenebis(salicylideneamine)), under acidic conditions gives H_2O and a deoxygenated lower-valent spieces (M^{X-2}(L)) which are reactive toward O_2, allowing the catalytic electroreduction of O_2 to H_2O.[3a] On the other hand, it has been reported that the autoxidation of [Fe^{II}(tpp)] produces μ-oxo iron(III) dimer (**II**). The reactivity of [Fe(tpp)] toward O_2, with significant potential in leading to the selective four-electron reduction of O_2 to H_2O, prompted the study on the reaction of **II** with an acid. The product for the acidification of CH_2Cl_2 solutions of **II** with an equimolar amount of perchloric acid was [(tpp)Fe^{III}(OH)] (**III**) and [(tpp)Fe^{III}(ClO$_4$)] (**IV**). The reaction believed to be responsible for the generation of **III** and **IV** is

$$[\{Fe(tpp)\}_2O] + HClO_4 \rightarrow [(tpp)Fe(OH)] + [(tpp)Fe(ClO_4)]. \quad (1)$$

Single crystals of the iron(III) complex (**IV**) were isolated from an acidified solution of **II** after layering with hydrocarbons. X-ray diffraction studies of the crystallized product revealed the formulation as Fe(tpp)(ClO$_4$)(*p*-xylene)$_{1.5}$ (Fig. 1). The structure consists of one [(tpp)Fe(ClO$_4$)] and 1.5 *p*-xylene solvate per asymmetric unit. The perchlorate ligand is monodentate with an unusually short Fe–O distance

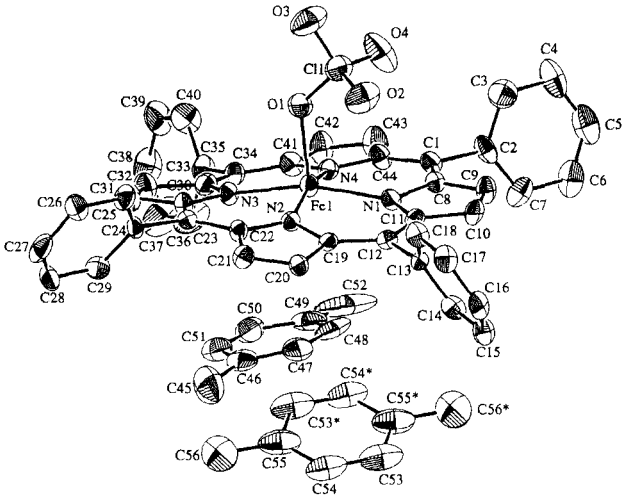

Fig. 1. ORTEP view (30% probability ellipsoids) of [(tpp)Fe(ClO$_4$)](xylene)$_{1.5}$ (**IV**).

(2.042(7) Å). Square-pyramidal five coordination is a common geometry for iron(III) porphyrins. The average Fe–N bond length is 2.01 Å with the iron(III) atom deviated by 0.276 Å from the porphyrin least-squares plane. Figure 1 also shows the arrangement of the lattice solvate. One solvate is at the center of symmetry; the other is located in closer proximity to the porphyrin with almost parallel arrangement. The closest distance between the iron atom and a *p*-xylene carbon atom is 3.56(1) Å. Thus, there appears to be a weak π complex formed between the *p*-xylene and the porphyrin complex, which has also been claimed to exist in toluene-solvated metalloporphyrin crystals.[14] The complex **III** has been reported previously.[15] The previous study[15] involved the reaction of iron powder, acetic acid and H_2tpp and a treatment with NaOH (Method 3 in Experimental Section). In the present study, the complex **III** was isolated from an acidified solution of **II** (Method 2). The complex **III** was also prepared by the reaction of [Fe^{II}(tpp)] with O_2 in the presence of an equimolar amount of a reducing agent under acidic conditions (Method 1). Introduction of O_2 to a dilute solution of [Fe(tpp)] in the presence of a large amount of acid and an equimolar amount of a reducing agent allowed Fe : O_2 = 2 : 1 stoichiometry to produce **III** in high yield. A μ-OH dimer may be produced under less acidic conditions.[15b]

Electrochemistry of Iron Porphyrins under Acidic Conditions. The electrochemistry of **II** in DMSO, DMF, and pyridine has been studied previously.[16] However, to our knowledge, there has been no study on the redox process of **II** in the presence of protons. In Fig. 2(a) is shown a cyclic voltammogram of the complex **II** in dichloromethane. No redox wave was observed in the potential range from +0.8 down to negative potentials of at least −0.6 V (vs. Ag/AgCl). This is in accordance with the previous study,[16] because the oxo-bridged dimer **II** was reduced to [Fe^{II}(tpp)] at potentials more negative than −0.93V. On the other hand, when a small amount of trifluoroacetic acid was added to the solution, a new distinct reduction and oxidation peak couple near 0 V (vs. Ag/AgCl) appeared (Fig. 2(b)). Despite the

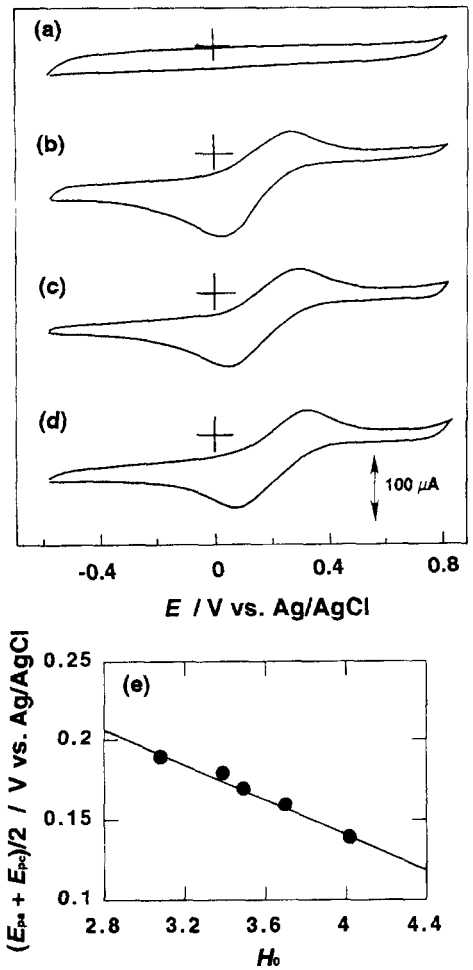

Fig. 2. Cyclic voltammograms for 0.5 mM of **II** in argon-saturated dichloromethane solution at a glassy carbon electrode ($A = 0.28$ cm^2) in the presence of (a) 0 mM, (b) 4.6 mM, (c) 9.3 mM, and (d) 14 mM CF_3COOH. (e) Dependence of redox potentials on Hammett acidity function H_0. The potentials corresponds to the average of the anodic and cathodic peak potential in the cyclic voltammograms. Supporting electrolyte was 0.1 M $TBABF_4$. Scan rate was 50 mV s^{-1}.

large peak potential separation due probably to the slow kinetics of the electrode reaction, the peaks are considered to be quasi-reversible, and could be appoximated by the Nernst equation. Indeed, by varying the potential sweep rate from 25 to 100 mV s^{-1}, the peak-to-peak separation in the cyclic voltammograms in Fig. 2 changed from 190 to 235 mV; the difference between the value of $(E_{pa}+E_{pc})/2$ obtained for the sweep rate of 100 and 25 mV s^{-1} was less than 10 mV, which may indicate that the value of $(E_{pa}+E_{pc})/2$ provides a good approximation of the formal potential. The peak potentials moved to more positive values with increasing the acidity (Figs. 2(c) and 2(d)).

In Fig. 2(e) is shown the acidity (indicated by the Hammett acidity function (H_0)) dependence of the potential. The linear plots with a slope close to 59 mV per H_0 unit indicates that one proton per electron is consumed during the reduction of **II**. The reduction of **II** to form two molecules of iron-(II) porphyrin was also supported by spectroelectrochemical measurements during the electrolysis of an argon-saturated acidic toluene solution of **II**. Figure 3 shows the UV spectra recorded during the electrolysis of **II** to [Fe(tpp)] in the presence of trifluoroacetic acid where a well-defined isosbestic point was observed. No change in the spectrum was observed before the electrolysis, indicating that the reaction 1 does not occur at a significant rate under these conditions. The electrolysis at −0.10 **V** (vs. Ag/AgCl) consumed two electrons per dimer and produced [Fe^{II}(tpp)] having the characteristic Soret band maximum at 432 nm.[17]

The chemical reduction by a reducing agent, such as sodium dithionite, was also employed to offer evidence for the formation of [Fe^{II}(tpp)]. In the absence of an acid, the complex **II** was not reduced to [Fe^{II}(tpp)], even in the presence of excess sodium dithionite. In contrast, [Fe^{II}(tpp)] was quantitatively produced in acidic media (see Experimental Section). Thus, the redox response recorded under acidic conditions is responsible for the reversible reduction of **II** to [Fe^{II}(tpp)], and the apparent formal potential for the quasi-Nernstian process obtained at 0.011 mM (1 M = 1 mol dm^{-3}) of **II** in CH_2Cl_2 is approximated by Eq. 2. This is not contradictory with the previous studies describing that the redox potential for [Fe(tpp)]$^{0/+}$ couple is near −0.19 V.[16a,17] The quasi-reversibility of the voltammogram in Fig. 2 would indicate that water molecules should be present in the electrolyte solution, which may be introduced with the addition of acid. The molecularity constraints of the reverse reaction suggest that the apparent formal potential should be a function of the concentration of both H_2O and [{Fe(tpp)}$_2$O]:

$$[\{Fe^{III}(tpp)\}_2O] + 2H^+ + 2e^- \rightarrow 2[Fe^{II}(tpp)] + H_2O; \quad (2)$$

at $E^f(\mathbf{II})_{app} = 0.38 - 0.059H_0$ (V vs. Ag/AgCl) in CH_2Cl_2.

An analogy to this and the following experimental results establish that the reaction 2 also takes place when the complex is adsorbed at the surface of the electrode. In Fig. 4(a) is shown the cyclic voltammograms obtained for the com-

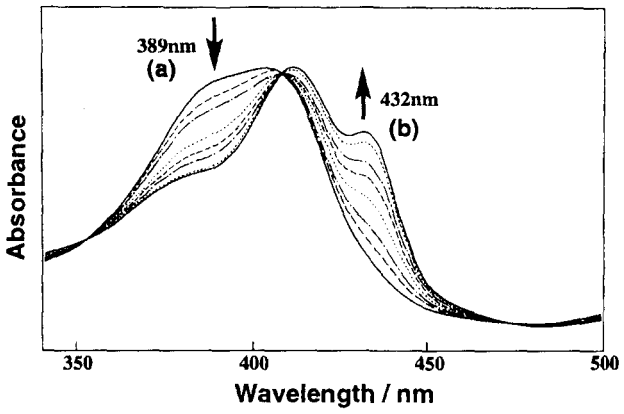

Fig. 3. UV-vis spectra recorded during the controlled-potential electroreduction of **II** at −0.10 V using a platinum mesh electrode. The electrolyte solution contained 0.011 mM of **II**, 0.1 M of $TBABF_4$ and 4.6 mM of CF_3COOH in toluene. Curve (a) corresponds to the spectrum before electrolysis, and curve (b) to that after electrolysis was completed.

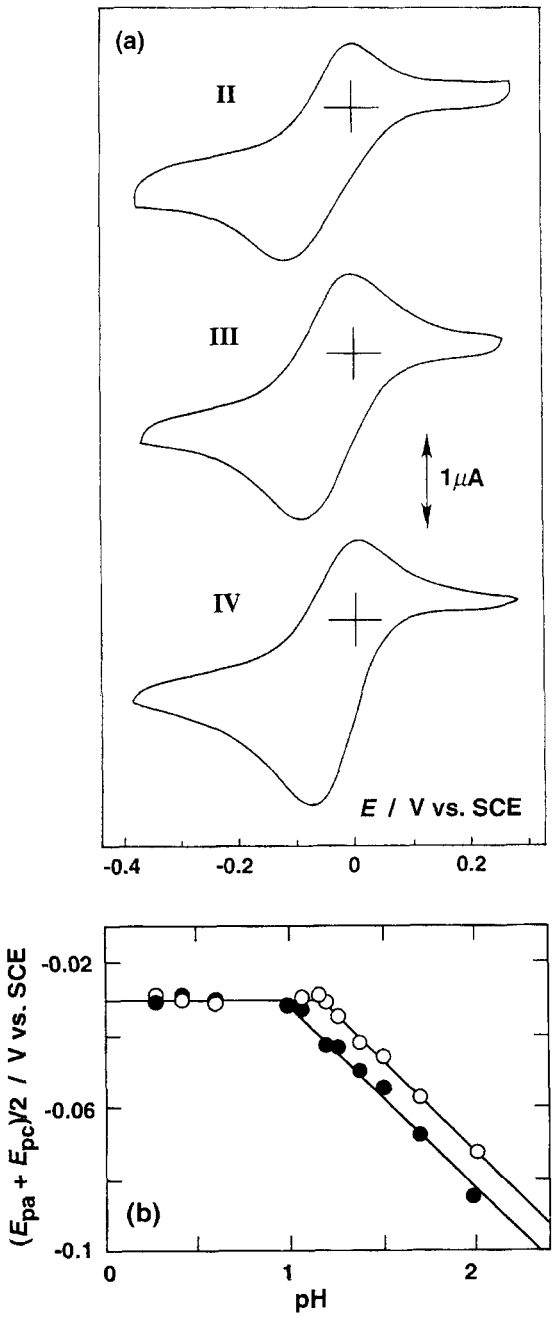

Fig. 4. (a) Cyclic voltammograms obtained with a glassy carbon electrode ($A = 0.28$ cm^2) coated with 5.0×10^{-9} mol cm^{-2} of **II**, **III**, and **IV**; the electrolyte solution contained 0.1 M NH_4PF_6 and 50 mM $HClO_4$ in H_2O saturated with argon. Potential sweep rate was 200 mV s^{-1}. (b) Dependence of redox potentials for **II** (●) and **III** (○) on pH; the electrolyte solution contained $HClO_4$ and 0.1 M NH_4PF_6 in H_2O saturated with argon.

plexes **II**, **III**, and **IV** when they were adsorbed on the surface of a glassy carbon electrode and immersed in acidic aqueous electrolyte solutions under argon. The oxidation peak in the cyclic voltammograms shown in Fig. 4(a) appeared only after the electrolyte solution was thoroughly deaerated, indicating the high reactivity of [Fe^{II}(tpp)] with O_2 under these conditions. The peak potential separation between oxidation and reduction in these voltammograms ranged from 80 to 110 mV for potential scan rates from 50 up to 200 mV s^{-1}. The shape of the cyclic voltammograms does not correspond to what is theoretically predicted for an adsorbed monolayer which shows the forward and reverse peaks at the same potential. According to the dimensionality of the molecules determined by X-ray analyses (**II**, ca. 6×6×5 Å^3; **IV**, ca. 6×6×2 Å^3), multiple layers are involved in the voltammograms. The peak potential for **II** and **III** shifted toward more positive values at lower pH. The linear plots with slopes near 59 mV per pH unit indicate that one proton per electron is consumed in the reduction of **II** and **III** on the electrode surface (Fig. 4(b)). The pH dependence of the peak potential for **IV** under the same conditions was identical to that of **III**. The half-reactions responsible for the reduction of **II** and **III** are:

$$[(tpp)Fe^{III}OFe^{III}(tpp)]_{ad}+2H^+ +2e^- \rightarrow 2[Fe^{II}(tpp)]_{ad}+H_2O; \quad (3)$$

at $E^f(\mathbf{II}_{ad})_{app} = 0.031 - 0.059\text{pH}$ (V vs. SCE, pH > 1.0).

$$[(tpp)Fe^{III}(OH)]_{ad} + H^+ + e^- \rightarrow [Fe^{II}(tpp)]_{ad} + H_2O; \quad (4)$$

at $E^f(\mathbf{III}_{ad})_{app} = 0.042 - 0.059\text{pH}$ (V vs. SCE, pH > 1.2).

$$[Fe^{III}(tpp)^+]_{ad} + e^- \rightarrow [Fe^{II}(tpp)]_{ad}; \quad (5)$$

at $E^f(\mathbf{IV}_{ad})_{app} = -0.029$ (V vs. SCE, pH < 1.2).

The proposed half-reaction 3 for the reduction of **II** adsorbed on the electrode surface was also supported by Raman spectroscopy. The peak at 360 cm^{-1} is ascribed to the Fe–O bond, which typically appears for the dimer **II** (Figs. 5(a) and 5(b)).[18] As expected, this peak became small upon reduction in acidic media in the absence of O_2 (Fig. 5(c)). The complex **III** was produced by soaking the electrode in an aqueous acidic solution saturated with O_2 containing sodium dithionite, which was indicated by the disappearance of the above two peaks and the appearance of a peak at 3456 cm^{-1} in the IR spectrum which could be ascribed to the stretching of the OH bond.[19] The complex **III** is also reduced by sodium dithionite under strongly acidic conditions. However, at pH>5 the reduction by sodium dithionite may be slow, and the complex **III** produced according to [*P*Fe^{II} Fe^{II}*P*]$_{ad}$+O_2+2H$^+$+2e$^-$ → [*P*Fe^{III}OH HOFe^{III}*P*]$_{ad}$ could be detected.

Catalytic Reduction of O_2 by the Adsorbed Iron Porphyrins. The reactivity of [Fe(tpp)] toward O_2 and the stoichiometry of half-reactions 3 and 4 are reminiscent of the electroreduction of O_2 to H_2O, which prompted the study on the catalytic reduction of O_2 using these complexes. The establishment of the reduction of μ-oxo iron(III) dimers to [Fe^{II}(tpp)] under acidic conditions leads to an estimate that two cofacially fixed iron(II) porphyrin molecules could be produced at the surface of the electrode when the adsorbed dimer was reduced under acidic conditions.

The iron(III) porphyrin complexes were adsorbed on the surface of the glassy carbon electrode by transferring a measured volume (5 μL) of 0.1 mM solutions of the complexes

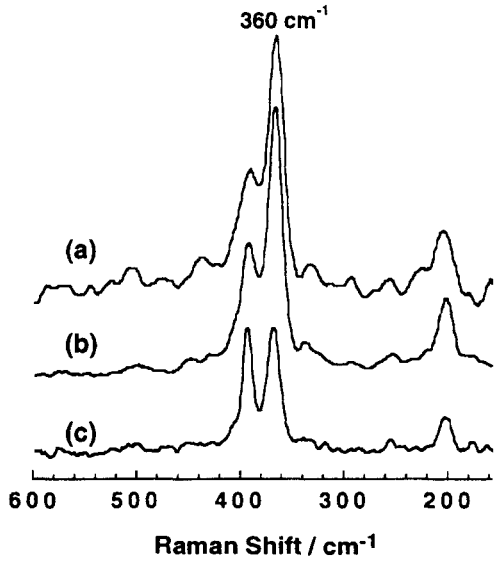

Fig. 5. Raman spectra of (a) crystals of **II**, and (b) the glassy carbon electrode coated with 5.0×10^{-9} mol cm^{-2} of **II**. (c) Repeat of (b) after the electrode was immersed in an aqueous electrolyte solution containing 0.1 M NH_4PF_6 and 0.5 M $HClO_4$ under argon and the adsorbate was reduced at −0.1 V. The spectra were obtained by 514.5 nm excitation.

in toluene. The solvent was allowed to evaporate at room temperature. The electrocatalytic behavior of O_2 reduction by the μ-oxo diiron(III) complexes **II** and **VI** adsorbed on the surface of glassy carbon electrode was examined by cyclic voltammetry. The cyclic voltammograms for the reduction of O_2 at the uncoated electrode are shown in Fig. 6(a). The presence of a quasi-reversible voltammetric response near 0.3 V (vs. SCE) is a feature common to all carbon electrodes.[20] The peak near −0.5 V (vs. SCE) corresponded to the direct reduction of O_2 at an uncoated carbon electrode. The dotted curve in Fig. 6(b) shows the typical current-potential responses obtained at a glassy carbon electrode adsorbed with **II** in argon-saturated aqueous acidic solutions. When the electrode was transferred to an O_2 saturated solution, a large catalytic current appeared near −0.22 V (vs. SCE). The second reduction peak near −0.5 V corresponds to the reduction of O_2 at an uncoated portion of the electrode surface. The cyclic voltammogram of the reduction of O_2 at a glassy carbon electrode coated with the complex **I** is shown in Fig. 6(c). The complexes **I** and **II** both showed rather unstable catalytic behavior for O_2 reduction; the catalytic current gradually decreased after the second scan in cyclic voltammetry. However, when the complex **VI** was adsorbed on the surface of the electrode, a more stable catalytic behavior near −0.07 V (vs. SCE) was observed, even after the 200th scan in cyclic voltammetry (Fig. 6(d)). It could be stated that OEP has a more planar structure compared with TPP, and hence the coordination and splitting reaction of the O_2 molecule by **VI** is made more feasible which should adhere to restricted dynamics in the adsorbed state. The potential where the complex **VI** operates as a catalyst was more positive than that for **II**, which is parallel to their intrinsic

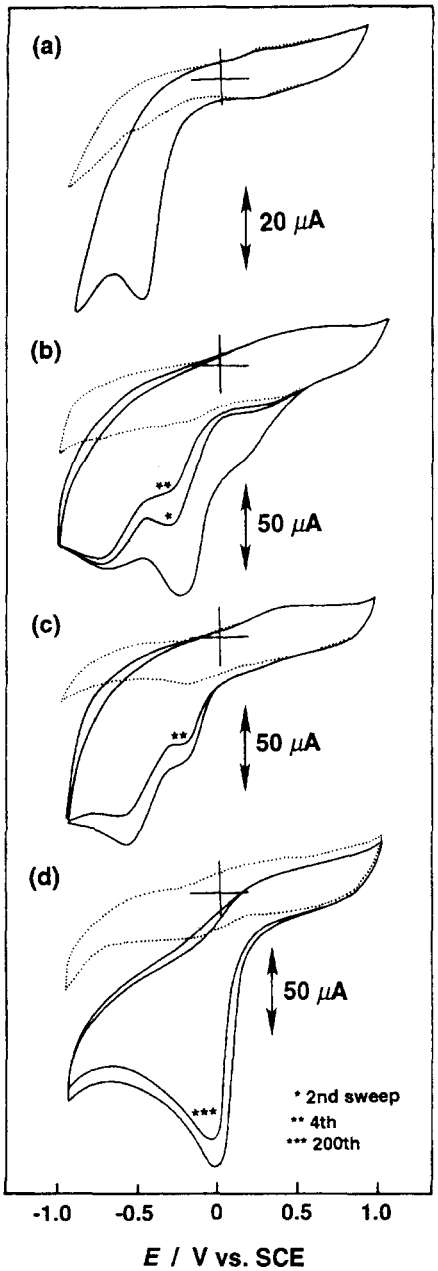

Fig. 6. Cyclic voltammograms obtained with (a) the bare glassy carbon electrode ($A = 0.28$ cm^2), and with the same electrode coated with (b) 6.8×10^{-3} mg cm^{-2} (5.0×10^{-9} mol cm^{-2}) of **II**; (c) 6.0×10^{-3} mg cm^{-2} (5.0×10^{-9} mol cm^{-2}) of **I**; (d) 3.5×10^{-3} mg cm^{-2} (5.0×10^{-9} mol cm^{-2}) of **VI**; the dotted curves were recorded under argon and the solid curves under O_2. The electrolyte solution contained 0.1 M NH_4PF_6 and 0.5 M $HClO_4$ in H_2O. Scan rate was 50 mV s^{-1}.

redox potentials.[21]

Quantitative kinetic data on the behavior of the catalysts were obtained by means of rotating disk voltammetry. Figure 7(a) shows a typical set of current–potential curves for **VI** for each electrode rotation rate. When these results are plotted as Koutecky–Levich plots (i_D^{-1} vs. $\omega^{-1/2}$, in Fig. 7(b)), the number of electrons (n) transferred in the O_2 reduction

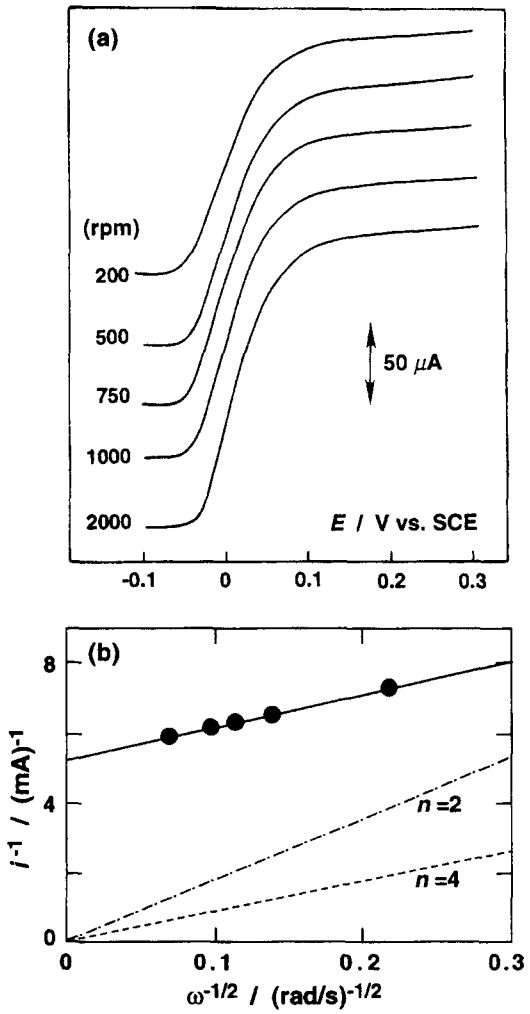

Fig. 7. (a) Rotating disk current-potential curves for electroreduction of O_2 at a glassy carbon electrode coated with **VI**. (b) Koutecky–Levich plots for the reduction of O_2 at a rotating glassy carbon disk electrode coated with **VI**. Other conditions were as in Fig. 6. The dashed line corresponds to the calculated response for the four-electron mass-transfer limited reduction.

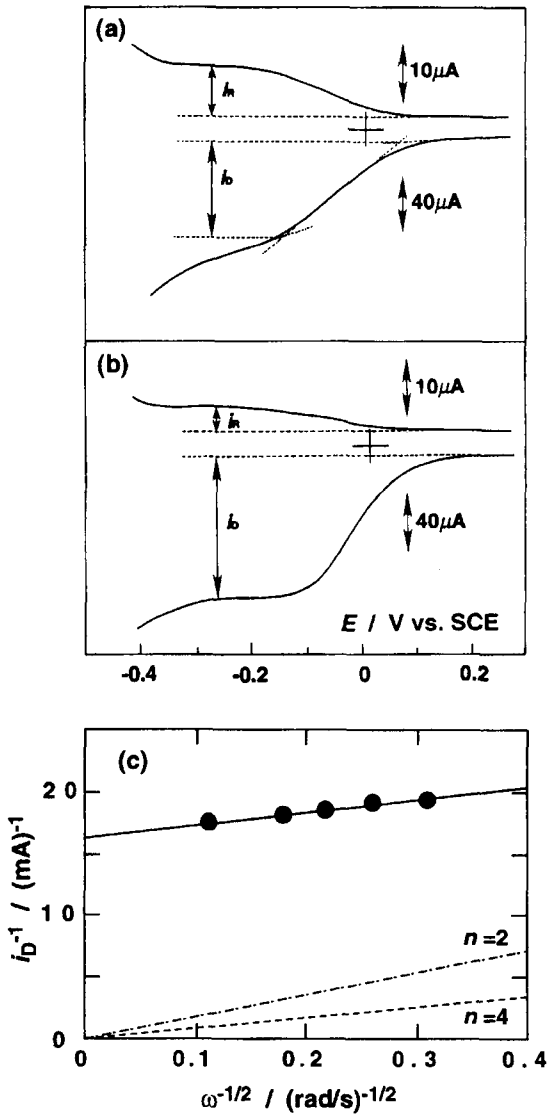

Fig. 8. Rotating ring-disk voltammogram using a platinum ring-glassy carbon disk electrode under O_2. Disk and ring currents were recorded vs the potential of the glassy carbon disk which was coated with (a) **I**, and (b) **II**. The platinum ring potential was maintained at +1.1 V. Electrode rotation rate was 500 rpm. (c) Koutecky–Levich plots for the reduction of O_2 at a rotating glassy carbon disk electrode coated with **II**. The other conditions were as Fig. 6.

can be determined.[22] From the slope of the plots, the value of n was evaluated to be 3.8 for the electrode coated with **VI**. The slope was quite similar to that of the dashed line calculated for the diffusion-limited four-electron reduction of O_2. The dimer **II** reduced O_2 with $n = 3.7$ with a significantly smaller magnitude of the kinetically limited current i_k (Fig. 8(c)). The mononuclear iron(III) porphyrin complexes **I** and **V** reduced O_2 with $n = 3.2$ and $n = 3.3$, respectively.

Rotating ring-disk voltammetry measurements were employed to provide support for the proposed four-electron reduction of O_2. The ring potential was maintained at 1.1 V to collect H_2O_2 which is produced by the two-electron reduction of O_2 at the disk electrode. When the disk was coated with the complex **II**, the ratio of the ring to disk currents was i_R/i_D ($= N$) = 0.026 (Fig. 8(b)). In comparison with the intrinsic value for the collection efficiency of the electrode determined by $Fe(CN)_6^{3-/4-}$ couple ($N_0 = 0.36$), the selectivity for the reaction where O_2 was reduced to H_2O directly by four-electron reduction ($(N_0-N)/(N_0+N)$) was evaluated to be 87%. The complex **VI** showed a higher selectivity for the four-electron reduction of O_2 (91%). These values are in good accordance with the slope of the Koutecky–Levich plots in Figs. 7(b) and 8(c). The observed ratio of ring to disk currents showed virtually no dependence on the electrode rotation rate, which could imply that a small amount of H_2O_2 is formed not as an intermediate, but as a parallel side product in O_2 reduction. On the other hand, no catalytic current was observed for the electroreduction of H_2O_2 using **II** in the same potential range. Thus, the four-electron reduction of O_2 by the μ-oxo iron(III) porphyrin dimer complexes would not

involve a mechanism in which H_2O_2 is an intermediate. In contrast, control experiments using a carbon electrode coated with the mononuclear complex **I** resulted in a more extensive formation of H_2O_2 ($i_R/i_D = 0.12$, at 500 rpm) under the same electrolyte conditions (Fig. 8(a)). The ratio of the ring to disk currents, normalized for the collection efficiency of the ring, corresponded to the reduction of 64% of the O_2 molecules to H_2O_2 under the same electrolyte conditions, which implies that the complex **I** was also a catalyst for the reduction of H_2O_2. The electrochemical data for the catalytic reduction of O_2 are summarized in Table 3.

The catalytic current for the reduction of O_2 by iron(III) porphyrins clearly depended on the quantity of the complexes (Γ) adsorbed on the electrode surface. Figure 9 shows the effect of Γ on the plateau current obtained with **V** and **VI**, respectively. As for the mononuclear complex **V**, the current for the O_2 reduction reached a maximum value when Γ was more than 6×10^{-10} mol cm^{-2}. According to X-ray analyses, the dimensionality of the molecule **V** was ca. $11\times11\times3$ Å^3 and that of **VI** was ca. $11\times11\times5$ Å^3. Because the geometric electrode area requires only ca. 1×10^{-10} mol cm^{-2} of the complex **V** to form a monolayer in a flat configuration, the complex **V** appears to form an aggregate on the surface of the electrode.[23] In contrast, the value of Γ required for the dinuclear complex **VI** (1.3×10^{-10} mol cm^{-2}) was much less than that for **V**. It appears that the μ-oxo iron(III) dimer has adsorption behavior on the electrode surface corresponding to that of a monolayer. In addition, the complex **VI** showed a higher selectivity for the four-electron reduction of O_2 than did the complex **V**, regardless of the quantity of the molecule at the electrode surface. It follows that two iron(II) porphyrin molecules, possibly in a face-to-face arrangement when they are produced by the electroreduction of the adsorbed μ-oxo dimer with the elimination of H_2O in aqueous acid, appear to play an essential role on the four-electron reduction of O_2. A more strongly adsorbing graphite electrode showed virtually identical behaviors, but a platinum electrode even adsorbed with the iron porphyrins showed only the reduction wave of protons under the acidic conditions.

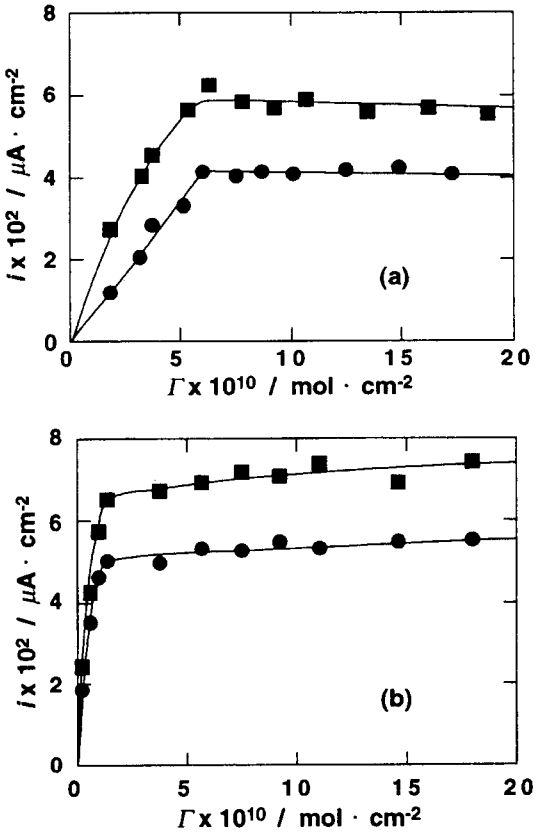

Fig. 9. Limiting disk currents for the reduction of O_2 at a rotating glassy carbon disk electrode on which increasing quantities of (a) **V** and (b) **VI** were coated. Electrode rotation rates were 200 rpm (●) and 1000 rpm (■), respectively. Other conditions were as Fig. 6.

Coordination and Splitting Mechanism of O_2. It has been suspected in the previous work[10] that a μ-O_2 iron(III) complex is formed as an intermediate during the course of the aerobic oxidation of [Fe^{II}(tpp)] to **II**. On the other hand, we have established that the reaction of [Fe^{II}(tpp)] with O_2 under acidic conditions in the presence of an equimolar amount of a reducing agent produces **III**, and that the electroreduction of **III** under acidic conditions produced H_2O and allowed a reformation of [Fe^{II}(tpp)]. It is quite clear from these results and those of Balch et al.[9,10] that involvement of the two iron porphyrins favors a four-electron reduction process of O_2 with O–O bond cleavage. Indeed, it is surprising that, when comparisons are made between the catalytic behavior of **I** and **II**, the μ-oxo bridge causes a significant increase in the selectivity of the four-electron pathway (Table 3). It may be safely stated that the cofacially oriented porphyrin molecules due to restricted dynamics of the adsorbate would allow accommodation of an O_2 molecule between the porphyrin planes and subsequent scission of the O–O bond. The catalytic reduction of O_2 proceeds at potentials in the vicinity of the reduction peak of **II** under acidic conditions. Thus, the contrast to the electroreduction of O_2 using mononuclear **I** originates from the capability to form two molecules of H_2O in the solid state upon the reaction with O_2. The catalytic mechanism is proposed to be as follows:

$$[P\mathrm{Fe^{II}}\ \mathrm{Fe^{II}}P]_{ad} + O_2 \rightarrow [P\mathrm{Fe^{III}}(O_2)\mathrm{Fe^{III}}P]_{ad} \quad (6)$$

$$[P\mathrm{Fe^{III}}(O_2)\mathrm{Fe^{III}}P]_{ad} \xrightarrow{+4H^+ +4e^-} [P\mathrm{Fe^{II}}\cdots OH_2\ H_2O\cdots \mathrm{Fe^{II}}P]_{ad} \xrightarrow[-2H_2O]{} [P\mathrm{Fe^{II}}\ \mathrm{Fe^{II}}P]_{ad} \quad (7)$$

The slow dynamics of the adsorbed porphyrin molecules is indicated by an independent experiments using (μ-peroxo)bis(phthalocyaninatoiron(III)) attached to an electrode, which shows quantitative O_2 coordination between the adjacent phthalocyanin molecules upon the reduction of iron(III) under acidic conditions repeatedly.[11b] The large displacement of the iron atoms from the porphyrin planes in μ-oxo dimers (**II**, 0.495 Å; **VI**, 0.490 Å) is likely to provide an adequate cavity for the accommodation of an O_2 molecule between the two iron atoms upon reduction (Fe^{II}–Fe^{II} distance = 4.5 Å, Fig. 10). However, the O_2-bridged intermediate complex has

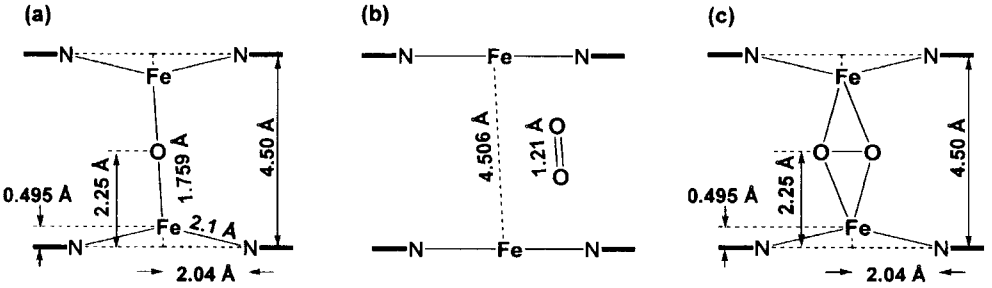

Fig. 10. Estimated structures of adsorbed porphyrins $[P\mathrm{Fe^{III}OFe^{III}}P]_{ad}$ (a), $[P\mathrm{Fe^{II}\,Fe^{II}}P]_{ad}$ (b), and $[P\mathrm{Fe^{III}(O_2)Fe^{III}}P]_{ad}$ (c). Parameters for (a) and (c) are from the crystal structures of **II**.

never been isolated in the case of iron; it is thus not known if it is a μ-$\eta^1:\eta^1$ complex or a μ-$\eta^2:\eta^2$ complex, the reason presumably being that the intermediate is highly reactive. On the other hand, the classical μ-$\eta^1:\eta^1$ complex is very well-known in the case of cobalt, but the reduction of O_2 through this complex proceeds to H_2O_2, except when the two cobalts are constrained in a very close face-to-face configuration, as discussed in the work of Collman et al.,[24] Le Mest et al.,[7a] and Chang et al.[7b] In this case, the μ-$\eta^2:\eta^2$ configuration is proposed to be responsible for the direct O_2 to H_2O conversion. Indeed, rationalization of the present results with those studies affords an indication in favor of the μ-$\eta^2:\eta^2$ configuration as follows: (1) In fact, the Fe–Fe distance which can be estimated from Fig. 10 is $2\times1.759=3.518$ Å, because the same out-of-plane displacement for any high-spin five-coordinate iron(III) is expected. (2) The cobalt–cobalt distance in the dicobalt cofacial porphyrins of Collman et al. is indeed 3.417 Å, according to the X-ray structure analysis.[25] (3) Theoretical studies, such as those of Hoffmann et al.[26] and of Le Mest et al.,[7a] demonstrate that the coordination of O_2 in a μ-$\eta^1:\eta^1$ configuration is strictly impossible in terms of orbital overlap with a metal–metal distance close to 3.5 Å. Conversely, such a short metal–metal distance is proposed to favor a μ-$\eta^2:\eta^2$ configuration and to considerably weaken the strength of the O–O bond. Indeed, the metal–metal distance found in the first discovered μ-$\eta^2:\eta^2$ dicopper compound[27] was almost the same value. It thus follows from the present results that such a type of coordination appears to be more appropriate, as proposed in Fig. 10(c). This is partly corroborated by the fact that the μ-oxo diiron(III) with TPP is less active than that with OEP, owing to a larger metal–metal distance due to steric repulsion.

In other studies, iron phthalocyanines incorporated in polypyrrole[28] and electropolymerized iron porphyrins[29] were also employed in attempts to allow the cofacial geometry. Simple μ-oxo dimers could be more convenient alternatives to the diporphyrins, despite the drawback that the corresponding μ-oxo dicobalt(III) complexes are not available. The present result would also lead to an estimate that μ-oxo dimers are versatile templates, leading to the face-to-face arrangement of a wide variety of metal complexes in the solid state, which could offer effective coordination sites for small molecules. Continuous research is underway in an attempt to allow the catalytic reduction of O_2 to occur at more positive potentials.

Experimental

Materials. 5,10,15,20-Tetraphenylporphine (H_2tpp) and 2,3,7,8,12,13,17,18-octaethylporphine (H_2oep) were obtained from Tokyo Kasei Co. *N*,*N*-Dimethyl formamide (DMF), toluene, and dichloromethane were purified by distillation in the usual manner. Tetrabutylammonium tetrafluoroborate was obtained from Wako Chem. Co. and recrystallized twice from a mixture of benzene and ethyl acetate. All other reagents were used as received.

(5, 10, 15, 20- Tetraphenylporphyrinato)iron(III) Chloride ([(tpp)FeCl], I). The complex **I** was prepared by the reaction of H_2tpp with $FeCl_2\cdot4H_2O$ in DMF under O_2 as an oxidant. UV-vis (λ_{max}/nm, ($10^{-4}\varepsilon$/M^{-1} cm^{-1}) in benzene) 380 (5.22) 417 (9.26), 508 (1.22), 577 (0.32). Anal. Calcd for $C_{44}H_{28}N_4FeCl$: C, 75.06; H, 4.00; N, 7.96%. Found: C, 75.32; H, 3.98; N, 8.20%.

(μ- Oxo)bis[(5, 10, 15, 20- tetraphenylporphyrinato)iron(III)] ([{Fe(tpp)}$_2$O], II). The complex **II** was prepared by the reaction of **I** in $CHCl_3$ with 25% aqueous KOH as described previously.[12] UV-vis (λ_{max}/nm, ($10^{-4}\varepsilon$/M^{-1} cm^{-1}) in benzene) 408 (18.1), 571 (1.57), 612 (0.69). IR (KBr): 891, 873 cm^{-1} ($\nu_{Fe-O-Fe}$). Anal. Calcd for $C_{88}H_{56}Fe_2N_8O$: C, 78.11; H, 4.17; N, 8.28%. Found: C, 77.88; H, 4.22; N, 7.60%. MS (FAB, *m*-nitrobenzyl alcohol matrix) Calcd for $C_{88}H_{56}Fe_2N_8O$: [M^+] (*m*/*z*) 1353. Found: *m*/*z* 1353, 1352.

(5, 10, 15, 20- Tetraphenylporphyrinato)iron(III) hydroxide ([(tpp)Fe(OH)], III). Method 1: Reaction of [Fe(tpp)] with O_2 in the Presence of Acid and an Equimolar Amount of a Reducing Agent. The complex **II** was reduced to [Fe^{II}(tpp)] by the following procedures. A 100-mL three-necked round-bottom flask equipped with an argon gas inlet, a rubber cork and an adapter joined to a 100-mL two-necked round-bottom flask containing anhydrous sodium sulfate was charged with **II** (50 μM) in a 20 mL toluene solution. An excess amount of trifluoroacetic acid (5 mM) in 10 mL toluene was degassed and added to the solution through a Teflon® tube. The mixture was stirred until the complex was completely dissolved. A 5-mL sodium dithionite aqueous solution (50 mM) was degassed and added to the reaction mixture through a Teflon® tube. The reaction mixture was stirred vigorously at room temperature for 20 min. The complex **II** in toluene was heterogeneously reduced by sodium dithionite in the H_2O layer. The color of the toluene layer in the reaction mixture gradually changed from violet to red. The toluene solution was extracted and subsequently dehydrated with anhydrous sodium sulfate under argon to provide [Fe^{II}(tpp)]. UV-vis (λ_{max}/nm, in toluene) 418, 442, 537 nm. The solvent was evaporated and replaced with CH_2Cl_2. The addition of O_2 to the solution of 50 μM [Fe^{II}(tpp)] in CH_2Cl_2 in the presence of 5 mM CF_3COOH and 50 μM sodium dithionite produced **III** quantitatively (94%). UV-vis (λ_{max}/nm, ($10^{-4}\varepsilon$/M^{-1} cm^{-1}) in benzene) 410 (12.47), 569 (1.01). IR (KBr) 3456 cm^{-1} (ν_{OH}).

There is no evidence for an oxo bridge, which displays an antisymmetric Fe–O–Fe stretching vibration at ca. 850 cm^{-1}. Anal. Calcd for $C_{44}H_{29}FeN_4O$: C, 77.08; H, 4.26; N, 8.17%. Found: C, 77.01; H, 4.21; N, 8.17%. D_{meas} ($g\,cm^{-3}$) 1.261±0.090. MS (FAB, *m*-nitrobenzyl alcohol matrix) Calcd for $C_{44}H_{29}FeN_4O$: [M^+] (*m/z*) 685, [M^+-OH] (*m/z*) 668. Found: *m/z* 685, 667. ESR (toluene, −150 °C): $g_\perp$ 5.6; $g_{//}$ 2.0. The absence of the Fe–O–Fe band in the IR spectrum and the determination of paramagnetic Fe(III) by the integration of the ESR spectrum preclude the contamination of the μ-oxo dimer **II** which is ESR silent due to the magnetic coupling through an oxo bridge.

Method 2: Acidification of CH_2Cl_2 Solution of II. The reaction of **II** in CH_2Cl_2 with an equimolar amount of perchloric acid offered an alternative method to prepare the complex **III**. The reaction produced a mixed solution of **III** and [(tpp)Fe(ClO_4)]. The complex **III** was isolated in low yield from the mixture by recrystallization from $CHCl_3$/*n*-hexane, providing fine crystals with essentially the same spectroscopic data.

Method 3: Hydrolysis of Porphyrinatoiron(III) Acetate. The complex **III** was also prepared by a procedure essentially identical to that described in the previous report.[12] A solution of iron(II) acetate in glacial acetic acid was added dropwise to the refluxing glacial acetic acid containing H_2tpp. The resulting [Fe(tpp)]($OCOCH_3$) was reacted with dilute aqueous sodium hydroxide at room temperature. A purification treatment was carried out by column separation. The product was identified as in Method 1.

(5,10,15,20-Tetraphenylporphyrinato)iron(III) Perchlorate ([(tpp)Fe(ClO_4)](p-xylene)$_{1.5}$, IV). The complex **IV** was prepared by a procedure essentially identical to that described in the literature.[14] Recrystallization of the product from $CHCl_3$/*p*-xylene gave single crystals suitable for X-ray diffraction experiments. UV-vis (λ_{max}/nm, ($10^{-4}\varepsilon/M^{-1}\,cm^{-1}$) in benzene) 400 (6.09), 526 (0.85). IR (KBr) 1181, 1109, 1090, 619 cm^{-1} (ν_{ClO_4}). Anal. Calcd for $C_{44}H_{32}ClFeN_4O_6$: C, 65.73; H, 4.01; N, 6.97%. Found: C, 66.34; H, 4.03; N, 6.32%. Acidification of the CH_2Cl_2 solution of **II** and recystallization of the product from $CHCl_3$/*p*-xylene also gave **IV** as single crystals having essentially the same structure.

(2,3,7,8,12,13,17,18-Octaethylporphyrinato)iron(III) Chloride ([(oep)FeCl], V). The complex **V** was prepared by the reaction of H_2oep with $FeCl_2\cdot 4H_2O$ in DMF under O_2 as an oxidant. UV-vis (λ_{max}/nm, ($10^{-4}\varepsilon/M^{-1}\,cm^{-1}$) in benzene) 374 (5.94), 401 (4.89), 533 (0.73), 632 (0.80). Anal. Calcd for $C_{36}H_{44}N_4FeCl$: C, 69.28; H, 7.11; N, 8.98%. Found: C, 69.22; H, 7.15; N, 9.09%.

(μ-Oxo)bis[(2,3,7,8,12,13,17,18-octaethylporphyrinato)iron(III)] ([{Fe(oep)}$_2$O], VI). The complex **VI** was prepared by the reaction of **V** in $CHCl_3$ with 25% aqueous KOH as described previously.[13] UV-vis (λ_{max}/nm, ($10^{-4}\varepsilon/M^{-1}cm^{-1}$) in benzene) 342 (7.65), 387 (11.95), 562 (1.35), 590 (1.12). IR (KBr) 837, 878 cm^{-1} ($\nu_{Fe-O-Fe}$). Anal. Calcd for $C_{72}H_{88}Fe_2N_8O$: C, 72.47; H, 7.43; N, 9.39%. Found: C, 72.41; H, 7.41; N, 9.39%. MS (FAB, *m*-nitrobenzyl alcohol matrix) Calcd for $C_{72}H_{88}Fe_2N_8O$: [M^+] (*m/z*) 1193. Found: *m/z* 1192, 1193.

Measurements. Electrochemical measurements were carried out in a conventional two-compartment cell. A glassy carbon disk-platinum ring was used as a working electrode and polished before each experiment with 0.05-μm alumina paste. The auxiliary electrode, a coiled platinum wire, was separated from the working solution by a fine-porosity frit. The reference electrode was a commercial SCE immersed in a salt bridge consisting of an aqueous solution of 0.1 M ammonium hexafluorophosphate, which was placed in the main cell compartment. The formal potential of the $Fe(CN)_6^{3-/4-}$ couple was 0.62 V vs. SCE. A commercial Ag/AgCl electrode immersed in a salt bridge consisting of 0.1 M tetrabutylammonium tetrafluoroborate was used for electrochemical measurements in organic solvents. A Nikko Keisoku DPGS-1 dual potentiogalvanostat and a Nikko Keisoku NFG-3 universal programmer were employed with a Graphtec WX2400 X–Y recorder to obtain the voltammograms. Coulometric exhaustive electrolysis was performed using a Nikko Keisoku NDCM-1 digital coulometer. The diffusion-limited currents for the reduction of O_2 in aqueous solutions at the rotating disk electrode were calculated using the following parameters: kinetic viscosity of H_2O at 25 °C, 0.010 $cm^2\,s^{-1}$; solubility of O_2 in saturated solutions, 1.3 mM; diffusion coefficient of O_2, 1.5×10^{-5} $cm^2\,s^{-1}$.[4,30] UV-vis spectra were obtained using a Shimadzu UV-2200 spectrophotometer. Infrared spectra were obtained using a JASCO FT-IR 5300 with potassium bromide pellets. Density measurements of the crystals were performed using a pycnometer. Raman spectra were obtained using a JASCO NRS-2000 laser Raman spectrometer. FABMS spectra were obtained using a VGZAB-HF spectrometer.

Determination of the Hammett Acidity Function (H_0). *m*-Nitroaniline (B) was used as a conventional indicator in CH_2Cl_2 solutions ([B] = 1.8×10^{-3} M). The addition of trifluoroacetic acid to the solutions produced the ammonium salt (HB^+). The concentration of HB^+ was determined from the absorbance in the UV spectra. The value of H_0 was determined using the following equa-

Table 1. Summary of X-Ray Crystallographic Data

Complex	[(tpp)Fe(ClO_4)](xylene)$_{1.5}$ (**IV**)		
Emp form	$C_{56}H_{43}ClFeN_4O_4$	Radiation	Mo $K\alpha$
Fw	927.28	Absn coeff μ	4.35 cm^{-1}
Cryst. syst.	Triclinic	$2\theta_{max}$/deg	50.0
Space group	$P\bar{1}$ (#2)	No. of reflns colld	7527
a/Å	11.909(3)	No. of unq reflns	7114
b/Å	19.603(4)	No. of obsd reflns	2611
c/Å	10.494(3)		($I>3.00\sigma(I)$)
α/deg	95.74(2)	Params	668
β/deg	107.91(2)	Refln/param ratio	3.91
γ/deg	89.14(2)	R	0.055
V/$Å^3$	2319.1(9)	R_w	0.050
Z	2	Goodness-of-fit	1.90
Density (calcd)	1.328 $g\,cm^{-3}$	Max peak in diff map	0.30 $e^-\,Å^{-3}$
Crystal size/mm	0.1×0.1×0.4	Min peak in diff map	−0.23 $e^-\,Å^{-3}$

Table 2. Selected Bond Lengths and Angles for [(tpp)-Fe(ClO_4)](xylene)$_{1.5}$ (**IV**) Characterized by X-Ray Crystallography[a)]

	[(tpp)Fe(ClO_4)](xylene)$_{1.5}$ (**IV**)		
Bond length			
Fe(1)–O(1)	2.042(7)	Fe(1)–N(1)	2.014(8)
Fe(1)–N(2)	2.010(8)	Fe(1)–N(3)	2.009(8)
Fe(1)–N(4)	2.005(8)	Cl(1)–O(1)	1.461(7)
Cl(1)–O(2)	1.398(8)	Cl(1)–O(3)	1.382(8)
Cl(1)–O(4)	1.42(1)		
Bond angle			
O(1)–Fe(1)–N(1)	101.9(3)	O(1)–Fe(1)–N(2)	95.5(3)
O(1)–Fe(1)–N(3)	95.1(3)	O(1)–Fe(1)–N(4)	99.1(3)
N(1)–Fe(1)–N(2)	89.4(3)	N(1)–Fe(1)–N(3)	163.0(3)
N(1)–Fe(1)–N(4)	88.7(3)	N(2)–Fe(1)–N(3)	89.2(3)
N(2)–Fe(1)–N(4)	165.4(3)	N(3)–Fe(1)–N(4)	88.4(3)
O(1)–Cl(1)–O(2)	109.2(5)	O(1)–Cl(1)–O(3)	107.4(5)
O(1)–Cl(1)–O(4)	105.7(5)	O(2)–Cl(1)–O(3)	112.5(6)
O(2)–Cl(1)–O(4)	110.6(6)	O(3)–Cl(1)–O(4)	111.2(7)
Fe(1)–O(1)–Cl(1)	131.6(4)		

a) Bond lengths are in angstroms. Bond angles are in degrees. Estimated standard deviations are given in parentheses.

Table 3. Summary of Electrochemical Data for the Catalytic Reduction of O_2 by Iron(III) Porphyrin Complexes

Complex[a)]	Abbr	$E_p(O_2)$[b)]	n[c)]	$4e^-$ selectivity[d)]
		V vs. SCE		%
[(tpp)FeCl]	(**I**)	−0.25	3.2	64
[{Fe(tpp)}$_2$O]	(**II**)	−0.22	3.7	87
[(oep)FeCl]	(**V**)	−0.09	3.5	68
[{Fe(oep)}$_2$O]	(**VI**)	−0.07	3.8	91

a) Adsorbed on a glassy carbon electrode (5.0×10^{-9} mol cm^{-2}). b) O_2 reduction peak potential in cyclic voltammetry. The electrolyte solution contained 0.1 M NH_4PF_6 and 0.5 M $HClO_4$ in H_2O which was continuously saturated with O_2. Scan rate = 50 mV s^{-1}. c) The number of electrons transferred in the O_2 reduction determined by the Koutecky–Levich plots. d) The selectivity for the reduction of O_2 to H_2O directly by four electrons.

tion: $H_0 = pK_a + \log\{[B]/[(HB^+)]\}$.

X-Ray Crystallography. Black prismatic crystals of **IV** were grown from chloroform solutions of the desired complex after layering with *p*-xylene. Following microscopic examination in air, a suitable crystal was mounted on a glass fiber at room temperature. All measurements were performed on a Rigaku AFC7R diffractometer with a 6.0 kW rotating anode generator and graphite monochromated Mo $K\alpha$ radiation (λ = 0.71073 Å). The unit cell parameters and the orientation matrix for data collection were determined by least-squares refinements using the setting angles of 25, carefully centered reflections in the range $20 < 2\theta < 25°$. The data were collected at a temperature using the ω–2θ scan technique to a maximum 2θ value of 55°. Scans were made at a speed of 8° min^{-1} (in omega). The weak reflections ($I < 10.0\sigma(I)$) were rescanned (up to 5 scans) and the counts were accumulated to ensure good counting statistics. Stationary background counts were recorded on each side of the reflection. The ratio of the peak counting time to the background counting time was 2 : 1. The diameter of the incident beam collimator was 1.0 mm. The crystal-to-detector distance was 258 nm, and the computer-controlled detector aperture was set to 9×13 mm (horizontal×vertical). The intensities of three representative reflections were measured after every 150 reflections. No decay correction was applied. The data were corrected for Lorentz and polarization effects.

Structure Solution and Refinement. The structure was solved by heavy-atom Patterson methods and expanded using Fourier techniques. The positions for most non-hydrogen atoms were visible on the initial *E*-map with positions of the remaining atoms found on subsequent electron density difference maps. The non-hydrogen atoms were refined anisotropically. All hydrogen atoms were refined isotropically. The final cycle of the full-matrix least-squares refinement[31] was based on the observed reflections ($I > 3\sigma(I)$), and converged with unweighted and weighted agreement factors of $R = \sum||F_o|-|F_c||/\sum|F_o|$ and $R_w = (\sum w(|F_o|-|F_c|)^2/\sum wF_o^2)^{1/2}$ as listed in Table 1. Plots of $\sum w(|F_o|-|F_c|)^2$ versus $|F_o|$, the reflection order in data collection, $\sin\theta/\lambda$ and various classes of indices showed no unusual trends. Data collection and structure solution parameters as well as the conditions are listed in Table 1. Selected bond lengths and angles are listed in Table 2. All calculations were performed using the teXsan crystallographic software package of Molecular Structure Corporation.[32] The anisotropic thermal parameters of non-hydrogen atoms and the atomic coordinates are deposited as Document No. 73025 at the Office of the Editor of Bull. Chem. Soc. Jpn. Crystallographic data have been deposited at the CCDC, 12 Union Road, Cambridge CB2 1EZ, UK and copies can be obtained on request, free of charge, by quoting the publication citation and the deposition numbers CCDC 140839.

The authors acknowledge discussions with Dr. Kimihisa Yamamoto of Keio University. This work was partially supported by Grants-in-Aid for Scientific Research (Nos. 11650878, 09555297, 09650982, and 085344) and the International Scientific Research Program (Joint Research No. 08044174) from the Ministry of Education, Science, Sports and Culture.

References

1 a) M. Yuasa, T. Nagaiwa, M. Kato, I. Sekine, and S. Hayashi, *J. Electrochem. Soc.*, **142**, 2612 (1995). b) J. A. R. van Veen, J. F. van Baar, and K. J. Kroese, *J. Chem. Soc., Faraday Trans. 1*, **77**, 2827 (1981). c) N. Kobayashi, M. Fujihira, K. Sunakawa, and T. Osa, *J. Electroanal. Chem.*, **101**, 269 (1979). d) T. Osaka, K. Naoi, T. Hirabayashi, and S. Nakamura, *Bull. Chem. Soc. Jpn.*, **59**, 2717 (1986).

2 a) S. Iwata, C. Ostermeier, B. Ludwig, and H. Michel, *Nature*, **376**, 660 (1996). b) T. Tsukihara, H. Aoyama, E. Yamashita, T. Tomizaki, H. Yamaguchi, K. Shinzawa-Itoh, R. Nakashima, R. Yaono, and S. Yoshikawa, *Science*, **269**, 1069 (1995).

3 a) K. Yamamoto, K. Oyaizu, and E. Tsuchida, *J. Am. Chem. Soc.*, **118**, 12665 (1996). b) K. Oyaizu, K. Yamamoto, K. Yoneda, and E. Tsuchida, *Inorg. Chem.*, **35**, 6634 (1996). c) K. Oyaizu and E. Tsuchida, *J. Am. Chem. Soc.*, **120**, 237 (1998). d) E. Tsuchida, K. Yamamoto, and K. Oyaizu, *J. Electroanal. Chem.*, **438**, 167 (1997). e) E. Tsuchida, K. Yamamoto, K. Oyaizu, F. Suzuki, H. Nishide, A. S. Hay, and Z. Y. Wang, *Macromolecules*, **28**, 409 (1995). f) E. Tsuchida, K. Yamamoto, K. Oyaizu, N. Iwasaki, and F. C. Anson, *Inorg. Chem.*, **33**, 1056 (1994). g) K. Yamamoto, E. Tsuchida, H. Nishide, M. Jikei, and K. Oyaizu, *Macromolecules*, **26**, 3432 (1993). h) E. Tsuchida, K. Yamamoto, M. Jikei, and H. Nishide, *Macromolecules*, **22**, 4138 (1989).

4 K. Kinoshita, "Electrochemical Oxygen Technology," John Wiley & Sons Inc., New York (1992).

5 J. H. Zagal, *Coord. Chem. Rev.*, **119**, 89 (1982).

6 a) K. Shigehara and F. C. Anson, *J. Phys. Chem.*, **86**, 2776 (1982). b) C. Shi and F. C. Anson, *Inorg. Chem.*, **29**, 4298 (1990).

7 a) Y. Le Mest, C. Inisan, A. Laouénan, M. L'Her, J. Talarmin, M. E. Khalifa, and J. Y. Saillard, *J. Am. Chem. Soc.*, **119**, 6095 (1997). b) C. K. Chang, H. Y. Liu, and I. Abdalmuhdi, *J. Am. Chem. Soc.*, **106**, 2725 (1984). c) J. P. Collman, P. S. Wagenknecht, and J. E. Hutchison, *Angew. Chem., Int. Ed. Engl.*, **33**, 1537 (1994). d) F. C. Anson, C. Shi, and B. Steiger, *Acc. Chem. Res.*, **30**, 437 (1997).

8 T. Sawaguchi, T. Matsue, K. Itaya, and I. Uchida, *Electrochim. Acta*, **36**, 703 (1991).

9 D. H. Chin, G. N. La Mar, and A. L. Balch, *J. Am. Chem. Soc.*, **102**, 4344 (1980).

10 D. H. Chin, G. N. La Mar, and A. L. Balch, *J. Am. Chem. Soc.*, **102**, 5947 (1980).

11 a) A. Haryono, K. Oyaizu, K. Yamamoto, J. Natori, and E. Tsuchida, *Chem. Lett.*, **1998**, 233. b) K. Oyaizu, A. Haryono, J. Natori, and E. Tsuchida, *J. Chem. Soc., Faraday Trans.*, **94**, 3737 (1998).

12 E. B. Fleischer and T. S. Srivastava, *J. Am. Chem. Soc.*, **91**, 2403 (1969).

13 B. Cheng, J. D. Hobbs, P. G. Debrunner, J. Erlebacher, J. A. Shelnutt, and W. R. Scheidt, *Inorg. Chem.*, **34**, 102 (1995).

14 C. A. Reed, T. Mashiko, S. P. Bentley, M. E. Kastner, W. R. Scheidt, K. Spartalian, and G. Lang, *J. Am. Chem. Soc.*, **101**, 2948 (1979).

15 a) E. B. Fleischer, C. K. Miller, and L. E. Webb, *J. Am. Chem. Soc.*, **86**, 2342 (1964). b) D. R. Evans, R. S. Mathur, K. Heerwegh, C. A. Reed, and Z. Xie, *Angew. Chem., Int. Ed. Engl.*, **36**, 1335 (1997).

16 a) K. M. Kadish, *Prog. Inorg. Chem.*, **34**, 435 (1986). b) K. M. Kadish, G. Larson, D. Lexa, and M. Momenteau, *J. Am. Chem. Soc.*, **97**, 282 (1975). c) S. E. Jones, G. S. Srivasta, D. T. Sawyer, and T. G. Traylor, *Inorg. Chem.*, **22**, 3903 (1983).

17 D. Lexa, M. Momenteau, and J. Mispelter, *Biochim. Biophys. Acta*, **338**, 151 (1974).

18 a) A. Takenaka, S. Takeuchi, Y. Kobayashi, and K. Itoh, *Surf. Sci.*, **158**, 359 (1985). b) F. Adar and T. S. Srivastava, *Proc. Natl. Acad. Sci. U.S.A.*, **72**, 4419 (1975).

19 C. Maricondi, W. Swift, and D. K. Straub, *J. Am. Chem. Soc.*, **91**, 5205 (1969).

20 a) K. F. Blurton, *Electrochim. Acta*, **18**, 869 (1973). b) B. D. Epstein, E. Dalle-Molle, and J. S. Mattson, *Carbon*, **9**, 609 (1971). c) J. R. Randin and E. Yeager, *J. Electroanal. Chem. Interfacial Electrochem.*, **58**, 313 (1975). d) J. F. Evans and T. Kuwana, *Anal. Chem.*, **49**, 1632 (1977).

21 a) R. H. Felton, in "The Porphyrins," ed by D. Dolphin, Academic Press, New York, Vol. V, Chap. 3. b) D. G. Davis, in "The Porphyrins," ed by D. Dolphin, Academic Press, New York, Vol. V, Chap. 4.

22 a) V. G. Levich, "Pysicochemical Hydrodynamics," Prentice Hall, Englewood Cliffs, NJ (1962). b) J. Koutecky and V. G. Levich, *Zh. Fiz. Khim.*, **32**, 1565 (1956).

23 W. I. White, in "The Porphyrins," ed by D. Dolphin, Academic Press, New York (1978), Vol. V.

24 J. P. Collman, P. Denisevich, Y. Konai, M. Marrocco, C. Koval, and F. C. Anson, *J. Am. Chem. Soc.*, **102**, 6027 (1980).

25 K. Kim, J. P. Collman, and J. A. Ibers, *J. Am. Chem. Soc.*, **110**, 4242 (1988).

26 K. Tatsumi and R. Hoffmann, *J. Am. Chem. Soc.*, **103**, 3328 (1981).

27 N. Kitajima, K. Fujisawa, and Y. Moro-oka, *J. Am. Chem. Soc.*, **111**, 8975 (1989).

28 a) A. Elzing, A. Van Der Putten, W. Visscher, and E. Barendrecht, *J. Electroanal. Chem.*, **233**, 113 (1987). b) K. Hanabusa, X. Ye, T. Koyama, A. Kurose, and H. Shirai, *Polym. J.*, **24**, 485 (1992).

29 D. Ozer, R. Harth, U. Mor, and A. Bettelheim, *J. Electroanal. Chem.*, **266**, 109 (1989).

30 D. R. Lawson, L. D. Whiteley, C. R. Martin, M. N. Szentirmay, and J. I. Song, *J. Electrochem. Soc.*, **135**, 2247 (1988).

31 Least-squares: Function minimized: $\sum w(|F_o| - |F_c|)^2$, where $w = (\sigma(F_o)^2 + (0.020(F_o))^2)^{-1}$.

32 "teXsan: Crystal Structure Analysis Package," Molecular Structure Corporation (1985 & 1992).